Calibration of atomic trajectories in a large-area dual-atom-interferometer gyroscope

Zhan-Wei Yao,[1,2] Si-Bin Lu,[1,3] Run-Bing Li,[1,2,*] Jun Luo,[1,2] Jin Wang,[1,2,†] and Ming-Sheng Zhan[1,2,‡]

[1]*State Key Laboratory of Magnetic Resonance and Atomic and Molecular Physics, Wuhan Institute of Physics and Mathematics, Chinese Academy of Sciences, Wuhan 430071, China*

[2]*Center for Cold Atom Physics, Chinese Academy of Sciences, Wuhan 430071, China*

[3]*School of physics, University of Chinese Academy of Sciences, Beijing 100049, China*

(Received 28 September 2017; revised manuscript received 11 December 2017; published 17 January 2018)

We propose and demonstrate a method for calibrating atomic trajectories in a large-area dual-atom-interferometer gyroscope. The atom trajectories are monitored by modulating and delaying the Raman transition, and they are precisely calibrated by controlling the laser orientation and the bias magnetic field. To improve the immunity to the gravity effect and the common phase noise, the symmetry and the overlap of two large-area atomic interference loops are optimized by calibrating the atomic trajectories and by aligning the Raman-laser orientations. The dual-atom-interferometer gyroscope is applied in the measurement of the Earth's rotation. The sensitivity is 1.2×10^{-6} rad s^{-1} $Hz^{-1/2}$, and the long-term stability is 6.2×10^{-8} rad/s at 2000 s.

DOI: 10.1103/PhysRevA.97.013620

I. INTRODUCTION

Gyroscopes have many important applications in scientific and technical fields [1–6]. As a novel rotation sensor, the atom-interferometer gyroscopes present ultrahigh sensitivity [7,8]. Because atom interferometers are both sensitive to the gravitational acceleration and the rotation, the gravity effect must be eliminated as much as possible in the rotation measurements. To cancel the gravity effect, the dual-atom-interferometer gyroscope has been designed and realized [8–13]. The sensitivity of an atom interferometer can be improved by enlarging the atomic interference area and suppressing the phase noise. The atomic interference area was enlarged by increasing the interrogation time between two consecutive Raman pulses [13,14]. The large-momentum-transfer beam splitters and mirrors were also developed by several groups, which is a potential technique for realizing a compact large-area atom-interferometer gyroscope. The large-area dual-atom-interferometer gyroscope has important potential applications in the field of geophysics [15,16]. Advances in the atom interferometer make it possible for a transportable atom-interferometer gyroscope [17].

However, the dual-atom-interferometer gyroscope is more sensitive to the gravity effect when the atomic interference area is enlarged. The symmetry and overlapping of atomic trajectories become very important to improve the performance of the dual-atom-interferometer gyroscope. If two atomic interference loops are not symmetrically overlapped, the gravity effect will cause a systematic error in the absolute rotation measurement. The phase noise, caused by the Raman lasers and the vibration, is also increased in a large-area atom interferometer. Thus, to improve the performance of the dual-atom-interferometer gyroscope, the symmetry and overlap of two large-area atomic interference loops must be optimized by calibrating the atom trajectories.

In this paper, we demonstrate the calibration of atomic trajectories in a large-area dual-atom-interferometer gyroscope. The atomic trajectories are monitored by modulating and delaying the Raman transition and are precisely calibrated by controlling the laser orientation and the bias magnetic field. The wave-vector orientation of the Raman beams is precisely aligned by controlling the mirrors with the piezoelectric transducer. After the wave-vector orientations are aligned and the atomic trajectories are well calibrated, the atom gyroscope is built based on two symmetric large-area atomic interference loops. The contrasts of two interference fringes are both larger than 20%, and each interference area is 20 mm^2. Here the calibration of the atomic trajectories is very important for suppressing the common phase noise and canceling the gravity-caused phase. Because the gravity-induced phase shifts have the same trends, they are canceled in two symmetric interference loops. The Earth's rotation is thus measured by extracting the differential phase.

II. EXPERIMENTAL SETUP

The schematic apparatus is shown in Fig. 1. The compact gyroscope is mounted on a vibration-isolated turntable. Similar to our previous work [18], the ^{85}Rb atoms are first loaded into two symmetric magneto-optical traps (MOTs) from the background vapor and are then launched by using the moving optical molasses technique, with a velocity of 2.5 m/s and at an angle of 14.0° with respect to the gravity direction. The polarization gradient cooling is applied when the atoms are accelerated from two MOTs. The cold atoms with the temperature of 5 μK are counterpropagating along the same parabolic trajectory. They are synchronously prepared to the initial state $|F = 2, m_F = 0\rangle$ by a microwave field and a blow-away laser. The initial atoms are manipulated by three pairs of separated Raman beams along the gravity direction. The resid-

*rbli@wipm.ac.cn
†wangjin@wipm.ac.cn
‡mszhan@wipm.ac.cn

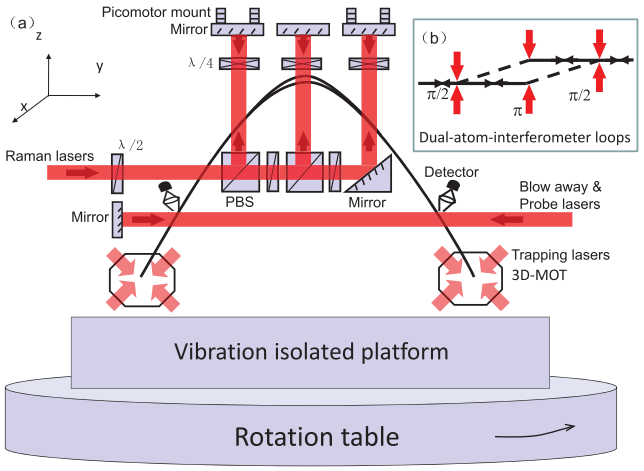

FIG. 1. Schematic diagram of experimental setup. An atom gyroscope is mounted on a vibration-isolated turntable. Three pairs of Raman laser beams are counterpropagating along the gravity direction for measuring the horizontal rotation component, and the symmetric dual-atom-interferometer loops are built by aligning the laser orientations and optimized by calibrating the atomic trajectories.

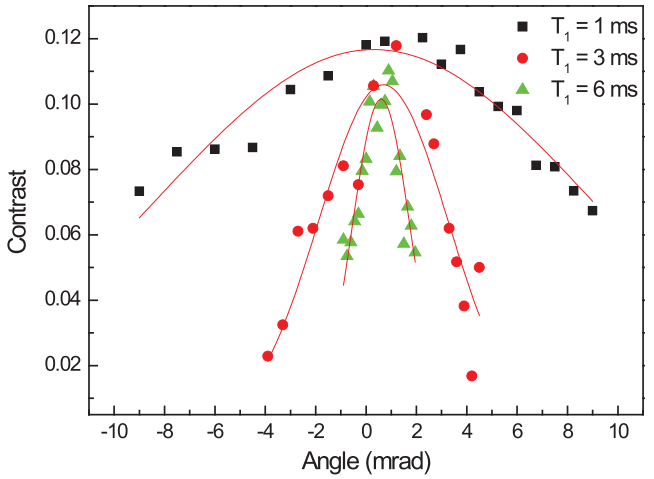

FIG. 2. The dependence of the contrast of Ramsey–Bordé fringes on the orientations between two consecutive Raman beams. The contrast depends on the alignment of Raman beams as the interrogation time increased.

ual magnetic field is compensated by three pairs of Helmholtz coils [19] and the ac Stark shift is canceled by adjusting the intensity ratio of the Raman beams [20]. The population of the state $|F = 3, m_F = 0\rangle$ is detected by the laser-induced fluorescence, and the atomic interference fringes are observed by scanning the differential phase of Raman lasers.

The Raman lasers are prepared with an optical phase-locked loop [21]. The frequency difference of the Raman lasers is 3.035 GHz, which corresponds to the clock transition of ^{85}Rb atoms. The main laser is locked to the transition between $|5S_{1/2}, F = 3\rangle$ and $|5P_{3/2}, F = 4\rangle$ by using the modulation transfer spectroscopy [22], and its frequency is redshifted by an acoustic-optic modulator (AOM, 200 MHz) with a four-pass configuration [23]. The slave laser and the main laser are combined together with a polarization beam splitter (PBS), and the beat-note signal is detected by a high-speed photodetector (Hamamatsu, G4176). To get the error signal and extend the frequency capture range, the beat-note signal is detected by a phase frequency discriminator (Analog Device, AD9901). The phase error is fed back to the current controller of the slave laser via a fast phase-locking module (Toptica, mFALC). The frequency is chirped at 2.5 MHz/s to compensate for the Doppler shift induced by gravity. Two tapered amplifiers are used to increase the powers of the Raman lasers. The Raman lasers are transmitted by a polarization-maintaining fiber and are well collimated by an achromatic doublet lens with a focal length of 150 mm. The power of the Raman lasers after the fiber is 240 mW, and their $1/e^2$ diameters are 36 mm. The intensity ratio of the Raman lasers is 1 : 2 to cancel the ac Stark shift. The Raman beams are split into three paths by using $\lambda/2$ wave plates, PBSs, and mirrors. Three pairs of separated counterpropagating Raman beams are applied along the gravity direction to build two large-area Mach–Zehnder (M-Z) atom interference loops, as shown in Fig. 1. The Raman lasers are switched by an 80 MHz AOM with a double-pass configuration. The durations are 16 μs for the $\pi/2$ Raman pulses and 32 μs for the π pulse. The interrogation time between two consecutive Raman pulses is $T = 52$ ms in the M-Z atom interferometers.

To overlap the atomic wave packets well, three pairs of Raman beams should be precisely aligned at a level of several μrad in the M-Z interferometer [14]. The alignment is performed by using a symmetric Ramsey–Bordé (R-B) interferometer due to less stringent requirements for the adjustment compared with the M-Z interferometer. Two motor-driven mounts (New Focus, Picomotor) are used to adjust the mirrors. The mounts are remotely controlled by the piezo-electric transducer drivers. First, by using a corner cube and reflection of redirected light on a water surface, three pairs of Raman beams are aligned along the gravity direction. The crossing angles between the Raman beams and the gravity direction are less than several mrad. Second, the alignment between two consecutive Raman beams is adjusted by using two symmetric R-B interferometers. One symmetric R-B interferometer is built with four $\pi/2$ Raman pulses, where two Raman pulses with the interrogation time T_1 are applied by the left Raman beams and the other two pulses with the same interrogation time provided by the middle Raman beams. The contrast of the R-B interference fringes is shown in Fig. 2. This contrast depends on the alignment of the Raman beams and the interrogation time. This provides a criterion for aligning the relative orientations between the left and middle Raman beams. The alignment is optimized as the interrogation time is increased. With the similar method, the alignment between the middle and right Raman beams is optimized with another symmetric R-B interferometer. Finally, the alignment of three pairs of Raman beams is adjusted by using the third symmetric R-B interferometer. Here the first pulse is applied by the left Raman beams, the second and third pulses provided by the middle Raman beams, and the fourth pulse provided by the right Raman beams. As the interrogation time is increased, the alignment of three pairs of Raman beams is optimized, and the R-B interferometer is transformed to the M-Z interferometer.

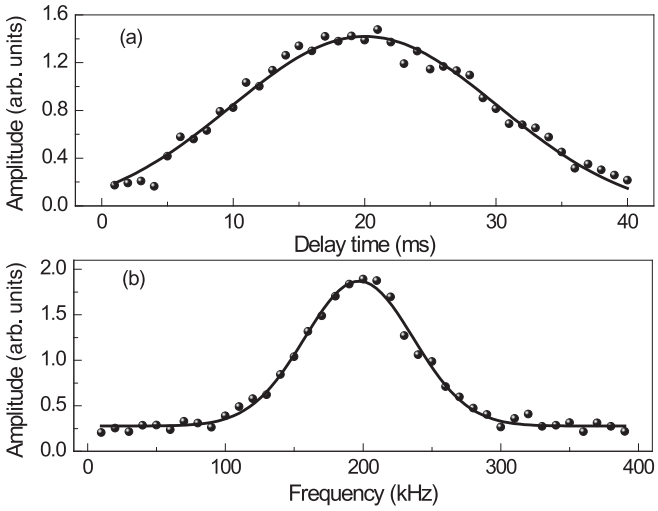

FIG. 3. The atomic trajectory measurement using the interaction between the atoms and the Raman beams. (a) Delaying the Raman pulse interaction time to measure the horizontal position. (b) Scanning the Raman transition to measure the vertical velocity.

III. CALIBRATION OF ATOM TRAJECTORIES

The M-Z atom interferometer is sensitive to rotation and gravity, and the phase shift caused by gravity and rotation is written as

$$\delta\varphi = \mathbf{k}_{\text{eff}} \cdot \mathbf{g}T^2 + 2\mathbf{k}_{\text{eff}} \cdot (\boldsymbol{\omega} \times \mathbf{v})T^2 + \phi_{\text{laser}}, \qquad (1)$$

where $\mathbf{k}_{\text{eff}}$ is the effective wave vector of the Raman beams, $\mathbf{g}$ is the gravitational acceleration, T is the interrogation time between two consecutive Raman pulses, $\boldsymbol{\omega}$ is the rotation rate of the frame, $\mathbf{v}$ is the velocity of atoms, and ϕ_{laser} is the phase of the Raman lasers. To measure the absolute rotation, the gravity effect should be eliminated as much as possible. In our experiment, two symmetric interference loops are built as shown in Fig. 1(b). Due to the inverse velocity, the rotation signal can be distinguished in dual-atom interferometers by subtracting their phase shifts. The rotation-induced phase shift $\delta\varphi_{\boldsymbol{\omega}}$ can be differentially measured as $4\mathbf{k}_{\text{eff}} \cdot (\boldsymbol{\omega}\times\mathbf{v})T^2$ according to Eq. (1). Furthermore, the common phase noise and the systematic error can be eliminated.

To decrease the systematic error and increase the contrast, the atomic trajectories of the dual-atom interferometer should be perfectly symmetric and overlapped. The atomic trajectories are calibrated by using the Raman transition. First, the atomic trajectories are monitored by the fluorescence signals of the Raman transition when one pair of counterpropagating Raman beams are applied. The atomic trajectories in different directions can be monitored by scanning the delay time and the two-photon detuning of the Raman lasers. Along the moving direction of the atoms, the atomic position is measured by controlling the delay time of the Raman pulse. By fitting the signal amplitude in Fig. 3(a) with a Gaussian function, the interaction time between the Raman lasers and the atom cloud is measured. In the vertical direction, we use the counterpropagating Raman transition to measure the atomic velocity. The Raman transition depends on the two-photon detuning as shown in Fig. 3(b). In the direction perpendicular to the atomic trajectory, the atomic position is measured by moving a slit which is mounted on a motorized translation stage (Thorlabs, MTS25) behind the Raman beams. These results give a judging criterion for calibrating the two atomic trajectories. In the gravity field, the trajectory of the atom cloud depends on its initial position, velocity, and orientation. During the moving molasses, the launch speed is controlled by the detuning of the cooling lasers, the launch angle is adjusted by the orientation of the cooling lasers, and the initial position of atom cloud is shifted by adjusting the bias magnetic field. Finally, the atomic trajectories are calibrated by adjusting their launch speeds and directions and optimized by monitoring the Raman transitions. After a series of modulations and measurements, two trajectories are overlapped in the horizontal and vertical directions and are made symmetric in the gravity direction. The position uncertainties in the horizontal and vertical directions are less than 0.08% and 0.10%, respectively. The atomic velocities along the gravity direction for each other are coincident with an uncertainty of 0.09%. The crossover between the copropagating and counterpropagating Raman transitions are avoided when the two atomic trajectories are perfectly optimized.

After the wave-vector orientations are aligned and the atomic trajectories are calibrated as mentioned in the previous sections, an atom gyroscope is built based on two symmetric large-area atomic interference loops. In the experiment, three pairs of separated Raman beams are used to build the M-Z interferometer. The $\pi/2$ pulses are applied by the left and right Raman beams, and the π pulses are provided by the middle Raman beams. Due to the precise alignment of the three pairs of Raman beams, the atomic wave packets can be well overlapped when the Raman-pulse sequences ($\pi/2$-π-$\pi/2$) are applied. The interrogation time between two consecutive pulses is achieved to be $T = 52$ ms in the M-Z interferometer. The two symmetric large-area atomic interference loops are built after the Raman-pulse sequence ($\pi/2$-π-$\pi/2$) is used to manipulate the atomic wave packets. The area is 20 mm^2 for each atomic interference loop. By optimizing the symmetry of two atomic interference loops, the contrast of atomic interference fringes is increased from 4% to more than 20%. Figure 4 shows the M-Z interference fringes with contrasts as 21.7% and 22.7%, respectively. The contrasts of two fringes are slightly different, which is mainly caused by the imbalance of three Raman pairs. Although the vibration causes phase noise in each atomic interference fringe, the differential phase noise can be suppressed in the dual atom interferometers.

IV. PERFORMANCE EVALUATION

The orientation of the Raman beams drifts with the temperature [24]. In the dual-atom-interferometer gyroscope, the initial phases are extracted from atomic interference fringes, and they show a long-term drift caused by the temperature. The phases are seriously drifted as shown in Figs. 5(a) and 5(b). According to Eq. (1), the rotation information is related to the differential phase between two atom interferometers as shown in Fig. 5(c). The drifts are canceled in the symmetric dual-atom interferometers, thus the absolute rotation can be measured.

Although this long-term drift can be canceled in the dual-atom interferometers, it is necessary to suppress this drift in

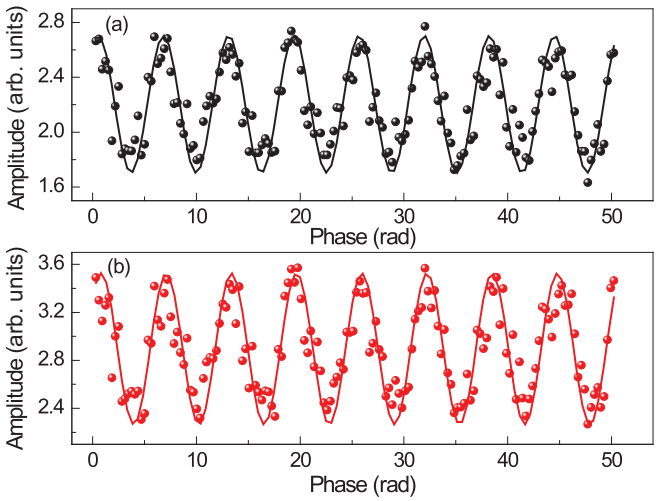

FIG. 4. The Mach–Zehnder fringes of the dual-atom interferometers. The contrasts are 21.7% for the first interferometer and 22.7% for the second one, respectively.

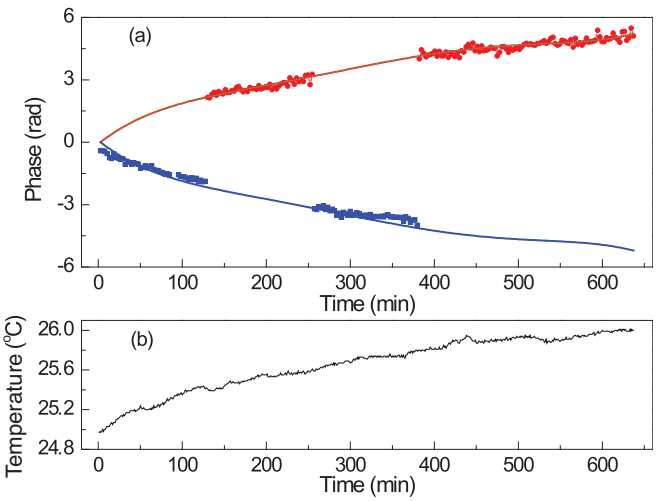

FIG. 6. The initial phase and the temperature drift of the atom interferometers. (a) The initial phases of the first atom interferometer with (red dots) and without (blue squares) reversing the wave vector. (b) The temperature drift.

each atom interferometer [25]. We synchronously monitor the temperature drift and the phase shifts of the dual-atom interferometers. The phase shift of the first atom interferometer is shown in Fig. 6(a), and the temperature drift is shown in Fig. 6(b). The temperature drift causes a gravity-like phase shift in each atom interferometer. The phase is increased when the Raman lasers are propagating along the gravity (red dots) and decreased when the Raman wave vector is reversed (blue squares). The phase drift is inverse as the wave vector of the Raman lasers reversed, and the Pearson correlation coefficient between the phase shift and the temperature drift is 0.99. The wave-vector reversal method can eliminate the residual phase shift, including the wavefront, the Zeeman effect, and the ac Stark effect.

The performance of rotation measurements is evaluated by the Allan deviation [26]. To reduce the amplitude noise and shorten the sampling time, the square-wave modulation is used to analyze the data [25]. The interference signal is set to two adjacent mid-fringe points by adjusting the phase difference of the Raman lasers. The populations $P(\psi)$ and $P(\psi+\pi)$ are measured, and the common noise is suppressed by subtracting $P(\psi)$ from $P(\psi+\pi)$. The vibration noise and the laser phase noise are differentially rejected in the dual-atom interferometers. To resolve the gravity drift, a feedback loop is applied, where the added signals $P(\psi)+P(\psi+\pi)$ are timely fed back to the Raman lasers. The subtracted signals $P(\psi)-P(\psi+\pi)$ give the rotation information. Figure 7

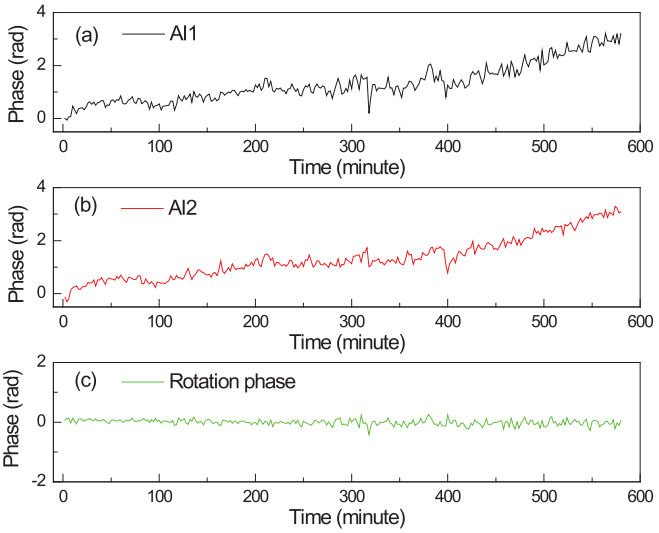

FIG. 5. The dependence of the phase drift on time. (a) The initial phases of the first atom interferometer. (b) The initial phases of the second atom interferometer. (c) The differential phase of the dual-atom interferometers.

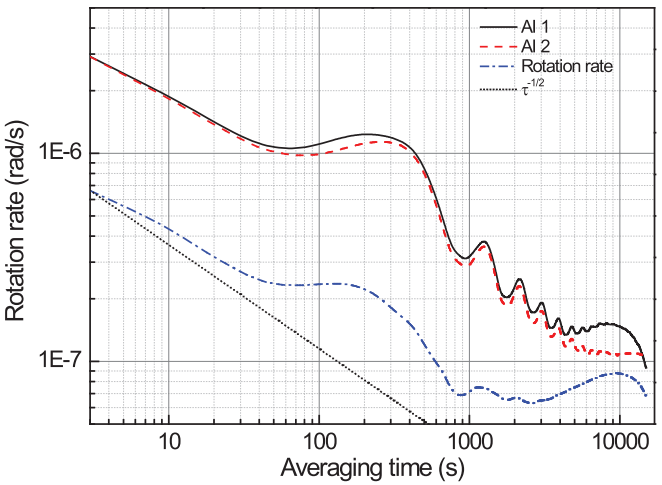

FIG. 7. The Allan deviations and the differential Allan deviation of the atom interferometers. The black solid line is for the first atom interferometer, and red dashed line is for the second one. The blue dot-dashed line is the differential Allan deviation for the dual-atom interferometers.

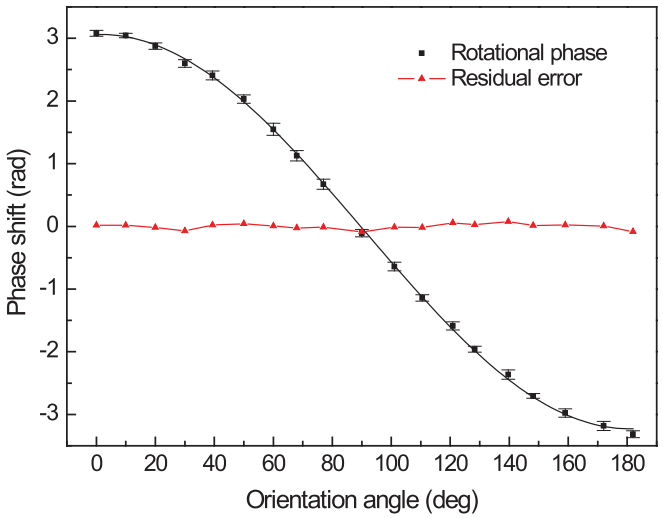

FIG. 8. The measurements of the Earth's rotation rate by modulating the turntable. The rotation-induced phase shift depends on the sensor orientation angle in laboratory coordinates, and it is a sinusoidal function.

shows the Allan deviations for the first (black solid line) and the second interferometer (red dashed line).

The temperature-induced phase drift is also compensated in both interferometers by the feedback loop. The differential Allan deviation between two atom interferometers is also shown in Fig. 7 (blue dot-dashed line), where the white noise is better suppressed. The humps in the individual Allan deviation curves are caused by the temperature oscillations, and they are suppressed in the differentially extracted gyroscope signal curve by using the feedback loop. The sensitivity of the atom gyroscope is 1.2×10^{-6} rad s^{-1} $Hz^{-1/2}$, and the long-term stability is 6.2×10^{-8} rad/s over the time of 2000 s.

V. ABSOLUTE ROTATION MEASUREMENT

The absolute rotation measurement will have important applications in inertial navigation, precision measurement, and in geophysics. To measure the absolute rotation rate for Earth, the experimental setup is mounted on an air-bearing turntable, which is driven by a direct-torque motor. The rotation angle of the turntable is calibrated by a precision goniometer (Renishaw RESM). The atomic interference area is along the horizontal direction. The projection of Earth's rotation on the atomic interference area changes as the setup rotates. The Earth-rotation-induced phase shift is the differential phase of the dual atom interferometers, which is a sinusoidal function as shown in Fig. 8 (black squares). The Raman lasers with and without reversing wave vectors are used to improve the accuracy of the rotation measurement.

The Earth's rotation rate is extracted by fitting the curve (black line), and it is measured to be $(6.24 \pm 0.03) \times 10^{-5}$ rad/s. Considering the latitude in our location, the Earth's rotation rate is $(7.32 \pm 0.03) \times 10^{-5}$ rad/s, which is consistent with the value provided by the International Earth Rotation Service (IERS). The residual errors between the experimental data and the fitting results are shown in Fig. 8 (red triangles). These errors are mainly caused by the magnetic-field gradient, which causes the unbalanced phase rejections in the dual-atom interferometers. The uncertainty of Earth's rotation rate is 0.5% with the value predicted. This result provides a potential candidate for monitoring Earth's rotation rate and seeking the north orientation of Earth.

VI. CONCLUSION AND DISCUSSION

In conclusion, the symmetry and overlapping of atomic trajectories are very important to improve the performance of the large-area dual-atom-interferometer gyroscope. We demonstrated a method for precisely calibrating the atomic trajectories in the large-area dual-atom-interferometer gyroscope. The large-area dual-atom-interferometer loops were built after the relative orientations of Raman mirrors were precisely aligned with a piezo-electric transducer. The atomic trajectories were monitored by the Raman transitions and precisely calibrated by controlling the laser orientation and the bias magnetic field. The symmetry and overlap of two atom-interferometer loops were improved after the atomic trajectories were precisely calibrated. The common phase noise was suppressed, the gravity effect was canceled, and the temperature drift was compensated. The short-term sensitivity of atom gyroscope was measured to be 1.2×10^{-6} rad s^{-1} $Hz^{-1/2}$, the long-term stability was 6.2×10^{-8} rad/s after an integrating time of 2000 s. The performance was mainly limited by the amplitude noise, which could be improved by normalized detection. The Earth's rotation rate was measured by modulating a turntable and agrees well with the value predicted in the IERS. This work is helpful to develop a high-precision gyroscope, which can be used to monitor Earth's rotation rate, seek its north orientation, and to develop an inertial instrument.

From Eq. (1), the rotation-induced phase shift in the M-Z atom interferometer is proportional to the square of interrogation time between two consecutive Raman pulses. The M-Z interferometer is more sensitive to the external noise as the interrogation time is increased. In this work, the interrogation time was improved to $T = 52$ ms by using three pairs of separated Raman beams. The area of 20 mm^2 was achieved for each atomic interference loop. In the future, the interference area could be enlarged from the present value by using the large-momentum-transfer beam splitter and mirror with the composite-light-pulse sequences. As two interference loops are enlarged, in order to well cancel the phase noise and the long-term drift, it will be even more important to improve the symmetry and overlapping of atomic trajectories. This work provides a method for precisely calibrating the atomic trajectories, which is important to improve the performance of the dual-atom-interferometer gyroscope.

ACKNOWLEDGMENTS

We acknowledge the financial support from the National Key Research and Development Program of China under Grant No. 2016YFA0302002, the National Natural Science Foundation of China under Grants No. 91536221, No. 11674362, and No. 91736311, the Strategic Priority Research Program of Chinese Academy of Sciences under Grant No. XDB21010100, and the Youth Innovation Promotion Association of Chinese Academy of Sciences.

[1] G. E. Stedman, Ring-laser tests of fundamental physics and geophysics, Rep. Prog. Phys. **60**, 615 (1997).
[2] P. Brosche and H. Schuh, Tides and Earth rotation, Surv. Geophys. **19**, 417 (1998).
[3] N. Barbour and G. Schmidt, Inertial sensor technology trends, IEEE Sens. J. **1**, 332 (2002).
[4] I. Ciufolini and E. C. Pavlis, A confirmation of the general relativistic prediction of the Lense-Thirring effect, Nature (London) **431**, 958 (2004).
[5] G. Bernard, Solar time, legal time, time in use, Metrologia **48**, S181 (2011).
[6] H. Lefèvre, The fiber-optic gyroscope: Challenges to become the ultimate rotation-sensing technology, Opt. Fiber Technol. **19**, 828 (2013).
[7] M. O. Scully and J. P. Dowling, Quantum-noise limits to matter-wave interferometry, Phys. Rev. A **48**, 3186 (1993).
[8] T. L. Gustavson, A. Landragin, and M. A. Kasevich, Rotation sensing with a dual atom-interferometer Sagnac gyroscope, Classical Quantum Gravity **17**, 2385 (2000).
[9] B. Canuel, F. Leduc, D. Holleville, A. Gauguet, J. Fils, A. Virdis, A. Clairon, N. Dimarcq, C. J. Bordé, A. Landragin, and P. Bouyer, Six-Axis Inertial Sensor Using Cold-Atom Interferometry, Phys. Rev. Lett. **97**, 010402 (2006).
[10] A. Gauguet, B. Canuel, T. Lévèque, W. Chaibi, and A. Landragin, Characterization and limits of a cold-atom Sagnac interferometer, Phys. Rev. A **80**, 063604 (2009).
[11] J. K. Stockton, K. Takase, and M. A. Kasevich, Absolute Geodetic Rotation Measurement Using Atom Interferometry, Phys. Rev. Lett. **107**, 133001 (2011).
[12] A. V. Rakholia, H. J. McGuinness, and G. W. Biedermann, Dual-Axis High-Data-Rate Atom Interferometer Via Cold Ensemble Exchange, Phys. Rev. Appl. **2**, 054012 (2014).
[13] P. Berg, S. Abend, G. Tackmann, C. Schubert, E. Giese, W. P. Schleich, F. A. Narducci, W. Ertmer, and E. M. Rasel, Composite-Light-Pulse Technique for High-Precision Atom Interferometry, Phys. Rev. Lett. **114**, 063002 (2015).
[14] G. Tackmann, P. Berg, C. Schubert, S. Abend, M. Gilowski, W. Ertmer, and E. M. Rasel, Self-alignment of a compact large-area atomic Sagnac interferometer, New J. Phys. **14**, 015002 (2012).
[15] B. Barretta, R. Geiger, I. Dutta, M. Meunier, B. Canuel, A. Gauguet, P. Bouyer, and A. Landragin, The Sagnac effect: 20 years of development in matter-wave interferometry, C. R. Phys. **15**, 875 (2014).
[16] I. Dutta, D. Savoie, B. Fang, B. Venon, C. L. Garrido Alzar, R. Geiger, and A. Landragin, Continuous Cold-Atom Inertial Sensor with 1 nrad/sec Rotation Stability, Phys. Rev. Lett. **116**, 183003 (2016).
[17] M. Hauth, C. Freier, V. Schkolnik, A. Senger, M. Schmidt, and A. Peters, First gravity measurements using the mobile atom interferometer gain, Appl. Phys. B: Lasers Opt. **113**, 49 (2013).
[18] Z. W. Yao, S. B. Lu, R. B. Li, L. Cao, J. Wang, and M. S. Zhan, Continuous dynamic rotation measurements using a compact cold atom gyroscope, Chin. Phys. Lett. **33**, 083701 (2016).
[19] R. B. Li, P. Wang, H. Yan, J. Wang, and M. S. Zhan, Magnetic field dependence of coherent population transfer by the stimulated Raman transition, Phys. Rev. A **77**, 033425 (2008).
[20] R. B. Li, L. Zhou, J. Wang, and M. S. Zhan, Measurement of the quadratic Zeeman shift of ^{85}Rb hyperfine sublevels using stimulated Raman transitions, Opt. Commun. **282**, 1340 (2009).
[21] S. H. Yim, S. B. Lee, T. Y. Kwon, and S. E. Park, Optical phase locking of two extended-cavity diode lasers with ultra-low phase noise for atom interferometry, Appl. Phys. B: Lasers Opt. **115**, 491 (2014).
[22] D. J. McCarron, S. A. King, and S. L. Cornish, Modulation transfer spectroscopy in atomic rubidium, Meas. Sci. Technol. **19**, 105601 (2008).
[23] E. A. Donley, T. P. Heavner, F. Levi, M. O. Tataw, and S. R. Jefferts, Double-pass acousto-optic modulator system, Rev. Sci. Instrum. **76**, 063112 (2005).
[24] D. S. Durfee, Y. K. Shaham, and M. A. Kasevich, Long-Term Stability of an Area-Reversible Atom-Interferometer Sagnac Gyroscope, Phys. Rev. Lett. **97**, 240801 (2006).
[25] P. Cheinet, F. P. D. Santos, T. Petelski, J. L. Gouët, J. Kim, K. T. Therkildsen, A. Clairon, and A. Landragin, Compact laser system for atom interferometry, Appl. Phys. B: Lasers Opt. **84**, 643 (2006).
[26] C. N. Lawrence, and J. P. Darryll, Characterization of ring laser gyro performance using the Allan variance method, J. Guid. Control Dyn. **20**, 211 (1997).